Flexural-torsional coupled vibration and buckling of thin-walled open section composite beams using shear-deformable beam theory

Thuc Phuong Vo* and Jaehong Lee†

Department of Architectural Engineering, Sejong University
98 Kunja Dong, Kwangjin Ku, Seoul 143-747, Korea

(Dated: November 7, 2008)

A general analytical model based on shear-deformable beam theory has been developed to study the flexural-torsional coupled vibration and buckling of thin-walled open section composite beams with arbitrary lay-ups. This model accounts for all the structural coupling coming from the material anisotropy. The seven governing differential equations for coupled flexural-torsional-shearing vibration are derived from the Hamilton's principle. The resulting coupling is referred to as sixfold coupled vibration. Numerical results are obtained to investigate effects of shear deformation, fiber orientation and axial force on the natural frequencies, corresponding mode shapes as well as load-frequency interaction curves.

Keywords: Thin-walled composite beams; shear deformation; flexural-torsional-shearing vibration; load-frequency interaction curves.

I. INTRODUCTION

Fiber-reinforced composite materials have been used over the past few decades in a variety of structures. Composites have many desirable characteristics, such as high ratio of stiffness and strength to weight, corrosion resistance and magnetic transparency. Thin-walled structural shapes made up of composite materials, which are usually produced by pultrusion, are being increasingly used in many engineering fields. However, the structural behavior is very complex due to coupling effects as well as warping-torsion and thus, the accurate prediction of stability limit state and dynamic

*Graduate student

†Professor, corresponding author. Tel.:+82-2-3408-3287; fax:+82-2-3408-3331

; Electronic address: jhlee@sejong.ac.kr

characteristics is of the fundamental importance in the design of thin-walled composite structures. Moreover, it is well known that the classical laminated beam theory, based on Euler-Bernoulli hypothesis, is inaccurate for moderate length to thickness ratio and/or for highly anisotropic composite beams. Therefore, incorporation of shear deformation effects is a major issue in the analysis of thin-walled composite beams due to their lower transverse modulus compared to in-plane modulus.

The theory of thin-walled open section members made of isotropic materials was first developed by Vlasov [1] and Gjelsvik [2]. Up to the present, investigation into the stability and vibrational behavior of these members has received widespread attention and has been carried out extensively since the early works of Timoshenko [3,4] and Trahair [5]. Closed-form solution for the flexural, torsional natural frequencies and critical buckling loads of isotropic thin-walled beams are found in the literature. For thin-walled composite material, Chandra et al. [6] presented a free vibration analysis of coupled composite I-beams with couplings under rotation. In order to validate the theory, graphite-epoxy and kevlar-epoxy I-beams with bending-torsion coupling were fabricated using an autoclave molding technique and tested in an in vacuo rotor test facility for their vibration characteristics. Song and Librescu [7] focused on the formulation of the general dynamic problem of arbitrary thin-walled open section composite beams. Besides, the monograph of Librescu and Song [8] was concerned not only with the foundation and formulation of linear and nonlinear theories but also provided powerful mathematical tools to address issues of statics and dynamics of thin-walled composite beams. Kollar [9-11] presented the analysis of flexural-torsional buckling and vibration of thin-walled open section composite beams. Vlasov's classical theory of thin-walled beams was modified to include both the transverse shear and the restrained warping induced shear deformations. Qiao et al. [12] introduced analytical study for free vibration analysis of fiber-reinforced plastic composite cantilever I-beams. Della and Shu [13,14] provided not only a relevant survey on the available analytical models and numerical analyses for the free vibration of delaminated composite laminates but also presented an analytical solution to the free vibrations of beams with two overlapping delaminations under axial compressive loads. In their model, the delaminated beam was analyzed as seven interconnected Euler-Bernoulli beams.

For some practical applications, earlier studies have shown that the effect of axial force on the natural frequencies and mode shapes is significant. Although a large number of studies have been performed on the dynamic characteristics of axially loaded isotropic thin-walled beams, it should be noted that only a few deal with thin-walled composite structures with arbitrary lay-ups. A literature survey on the subject shows that there appear some works reported on the free vibration of axially loaded closed-section thin-walled composite beams. Many numerical techniques have been

used to solve the dynamic analysis of thin-walled composite beams. One of the most effective approach is to derive the exact stiffness matrices based on the solution of the differential equation of beam. Most of those studies adopted an analytical method that required explicit expressions of exact displacement functions for governing equations. Banerjee [15,16] applied the exact dynamic stiffness matrix to perform the free vibration analysis of axially loaded composite Timoshenko beams. Li et al. [17-19] developed the analytical solution to determine the flexure-torsion coupled dynamic responses of axially loaded thin-walled composite beam under concentrated, distributed time-dependent loads and external stochastic excitations. The influences of axial force, Poisson effect, axial deformation, shear deformation and rotary inertia were also discussed in their research. By using finite element method, Bank and Kao [20] analysed free and forced vibration of thin-walled fibre reinforced composite material beams by using the Timoshenko beam theory. The works of Cortinez, Piovan, Machado and coworkers [21-23] deserved special attention because they introduced a new theoretical model for the generalized linear analysis of thin-walled composite beams. This model allowed studying many problems of static's, free vibrations with or without arbitrary initial stresses and linear stability of composite thin-walled beams. Machado et al. [23] also investigated the dynamic stability of thin-walled composite beams under axial external force. The analysis was based on a small strain and moderate rotation theory, which was formulated through the adoption of a second-order displacement field. In their research [21-23], thin-walled composite beams for both open and closed cross-sections and the shear flexibility (bending, non-uniform warping) were incorporated. However, it was strictly valid for symmetric balanced laminates and especially orthotropic laminates. Recently, Kim et al.[24-26] evaluated not only the exact element stiffness matrix to perform the spatially coupled stability analysis of thin-walled composite beams under a compressive force but also dynamic stiffness matrix of thin-walled composite I-beam with arbitrary laminations.

In this paper, which is an extension of the author's previous works [27-30], flexural-torsional coupled vibration and buckling of thin-walled open section composite beams with arbitrary lay-ups is presented. This model is based on the first-order shear-deformable beam theory, and accounts for all the structural coupling coming from the material anisotropy. The seven governing differential equations for coupled flexural-torsional-shearing vibration are derived from the Hamilton's principle. The resulting coupling is referred to as sixfold coupled vibration. A displacement-based one-dimensional finite element model is developed to solve the problem. Numerical results are obtained to investigate the effects of shear deformation, fiber orientation and axial force on the natural frequencies, corresponding mode shapes as well as load-frequency interaction curves.

II. KINEMATICS

The theoretical developments presented in this paper require two sets of coordinate systems which are mutually interrelated. The first coordinate system is the orthogonal Cartesian coordinate system (x, y, z), for which the x- and y-axes lie in the plane of the cross section and the z axis parallel to the longitudinal axis of the beam. The second coordinate system is the local plate coordinate (n, s, z) as shown in Fig.1, wherein the n axis is normal to the middle surface of a plate element, the s axis is tangent to the middle surface and is directed along the contour line of the cross section. The (n, s, z) and (x, y, z) coordinate systems are related through an angle of orientation θ as defined in Fig.1. Point P is called the pole axis, through which the axis parallel to the z axis is called the pole axis.

To derive the analytical model for a thin-walled composite beam, the following assumptions are made:

1. The contour of the thin wall does not deform in its own plane.
2. Transverse shear strains $\gamma^{\circ}_{xz}, \gamma^{\circ}_{yz}$ and warping shear γ°_{ω} are incorporated. It is assumed that they are uniform over the cross-sections.
3. Each laminate is thin and perfectly bonded.
4. Local buckling is not considered.

According to assumption 1, the midsurface displacement components $\bar{u}, \bar{v}$ at a point A in the contour coordinate system can be expressed in terms of a displacements U, V of the pole P in the x, y directions, respectively, and the rotation angle Φ about the pole axis,

$$\bar{u}(s, z) = U(z)\sin\theta(s) - V(z)\cos\theta(s) - \Phi(z)q(s) \tag{1a}$$

$$\bar{v}(s, z) = U(z)\cos\theta(s) + V(z)\sin\theta(s) + \Phi(z)r(s) \tag{1b}$$

These equations apply to the whole contour. The out-of-plane shell displacement $\bar{w}$ can now be found from the assumption 2. For each element of middle surface, the midsurface shear strains in the contour can be expressed with respect to the transverse shear and warping shear strains.

$$\bar{\gamma}_{nz}(s, z) = \gamma^{\circ}_{xz}(z)\sin\theta(s) - \gamma^{\circ}_{yz}(z)\cos\theta(s) - \gamma^{\circ}_{\omega}(z)q(s) \tag{2a}$$

$$\bar{\gamma}_{sz}(s, z) = \gamma^{\circ}_{xz}(z)\cos\theta(s) + \gamma^{\circ}_{yz}(z)\sin\theta(s) + \gamma^{\circ}_{\omega}(z)r(s) \tag{2b}$$

Further, it is assumed that midsurface shear strain in $s - n$ direction is zero ($\bar{\gamma}_{sn} = 0$). From the definition of the

shear strain, $\bar{\gamma}_{sz} = 0$ can also be given for each element of middle surface as:

$$\bar{\gamma}_{sz}(s,z) = \frac{\partial \bar{v}}{\partial z} + \frac{\partial \bar{w}}{\partial s} \tag{3}$$

After substituting for $\bar{v}$ from Eq.(1) into Eq.(3) and considering the following geometric relations,

$$dx = ds\cos\theta \tag{4a}$$

$$dy = ds\sin\theta \tag{4b}$$

Displacement $\bar{w}$ can be integrated with respect to s from the origin to an arbitrary point on the contour,

$$\bar{w}(s,z) = W(z) + \Psi_y(z)x(s) + \Psi_x(z)y(s) + \Psi_\omega(z)\omega(s) \tag{5}$$

where Ψ_x, Ψ_y and Ψ_ω represent rotations of the cross section with respect to x, y and ω, respectively, given by:

$$\Psi_y = \gamma^\circ_{xz}(z) - U' \tag{6a}$$

$$\Psi_x = \gamma^\circ_{yz}(z) - V' \tag{6b}$$

$$\Psi_\omega = \gamma^\circ_{\omega}(z) - \Phi' \tag{6c}$$

When the transverse shear effect is ignored, Eq.(6) degenerates to $\Psi_y = -U'$, $\Psi_x = -V'$ and $\Psi_\omega = -\Phi'$. As a result, the number of unknown variables reduces to four leading to the Euler-Bernoulli beam model. The prime ($'$) is used to indicate differentiation with respect to z; and ω is the so-called sectorial coordinate or warping function given by

$$\omega(s) = \int_{s_\circ}^{s} r(s)ds \tag{7a}$$

The displacement components u, v, w representing the deformation of any generic point on the profile section are given with respect to the midsurface displacements $\bar{u}, \bar{v}, \bar{w}$ by assuming the first order variation of inplane displacements v, w through the thickness of the contour as:

$$u(s,z,n) = \bar{u}(s,z) \tag{8a}$$

$$v(s,z,n) = \bar{v}(s,z) + n\bar{\psi}_s(s,z) \tag{8b}$$

$$w(s,z,n) = \bar{w}(s,z) + n\bar{\psi}_z(s,z) \tag{8c}$$

where, $\bar{\psi}_s$ and $\bar{\psi}_z$ denote the rotations of a transverse normal about the z and s axis, respectively. These functions can be determined by considering that the midsurface shear strains γ_{nz} is given by definition:

$$\bar{\gamma}_{nz}(s,z) = \frac{\partial \bar{w}}{\partial n} + \frac{\partial \bar{u}}{\partial z} \tag{9}$$

By comparing Eq.(2) and (9), the function can $\bar{\psi}_z$ can be written as

$$\bar{\psi}_z = \Psi_y \sin\theta - \Psi_x \cos\theta - \Psi_\omega q \tag{10}$$

Similarly, using the assumption that the shear strain γ_{sn} should vanish at midsurface, the function $\bar{\psi}_s$ can be obtained

$$\bar{\psi}_s = -\frac{\partial \bar{u}}{\partial s} \tag{11}$$

The strains associated with the small-displacement theory of elasticity are given by

$$\epsilon_s(s,z,n) = \bar{\epsilon}_s(s,z) + n\bar{\kappa}_s(s,z) \tag{12a}$$

$$\epsilon_z(s,z,n) = \bar{\epsilon}_z(s,z) + n\bar{\kappa}_z(s,z) \tag{12b}$$

$$\gamma_{sz}(s,z,n) = \bar{\gamma}_{sz}(s,z) + n\bar{\kappa}_{sz}(s,z) \tag{12c}$$

$$\gamma_{nz}(s,z,n) = \bar{\gamma}_{nz}(s,z) + n\bar{\kappa}_{nz}(s,z) \tag{12d}$$

where

$$\bar{\epsilon}_s = \frac{\partial \bar{v}}{\partial s}; \quad \bar{\epsilon}_z = \frac{\partial \bar{w}}{\partial z} \tag{13a}$$

$$\bar{\kappa}_s = \frac{\partial \bar{\psi}_s}{\partial s}; \quad \bar{\kappa}_z = \frac{\partial \bar{\psi}_z}{\partial z} \tag{13b}$$

$$\bar{\kappa}_{sz} = \frac{\partial \bar{\psi}_z}{\partial s} + \frac{\partial \bar{\psi}_s}{\partial z}; \quad \bar{\kappa}_{nz} = 0 \tag{13c}$$

All the other strains are identically zero. In Eq.(13), $\bar{\epsilon}_s$ and $\bar{\kappa}_s$ are assumed to be zero, and $\bar{\epsilon}_z$, $\bar{\kappa}_z$ and $\bar{\kappa}_{sz}$ are midsurface axial strain and biaxial curvature of the shell, respectively. The above shell strains can be converted to beam strain components by substituting Eqs.(1), (5) and (8) into Eq.(13) as

$$\bar{\epsilon}_z = \epsilon_z^\circ + x\kappa_y + y\kappa_x + \omega\kappa_\omega \tag{14a}$$

$$\bar{\kappa}_z = \kappa_y \sin\theta - \kappa_x \cos\theta - \kappa_\omega q \tag{14b}$$

$$\bar{\kappa}_{sz} = \kappa_{sz} \tag{14c}$$

where $\epsilon_z^\circ, \kappa_x, \kappa_y, \kappa_\omega$ and κ_{sz} are axial strain, biaxial curvatures in the x- and y-direction, warping curvature with

respect to the shear center, and twisting curvature in the beam, respectively defined as

$$\epsilon_z^\circ = W' \tag{15a}$$

$$\kappa_x = \Psi_x' \tag{15b}$$

$$\kappa_y = \Psi_y' \tag{15c}$$

$$\kappa_\omega = \Psi_\omega' \tag{15d}$$

$$\kappa_{sz} = \Phi' - \Psi_\omega \tag{15e}$$

The resulting strains can be obtained from Eqs.(12) and (14) as

$$\epsilon_z = \epsilon_z^\circ + (x + n\sin\theta)\kappa_y + (y - n\cos\theta)\kappa_x + (\omega - nq)\kappa_\omega \tag{16a}$$

$$\gamma_{sz} = \gamma_{xz}^\circ \cos\theta + \gamma_{yz}^\circ \sin\theta + \gamma_\omega^\circ r + n\kappa_{sz} \tag{16b}$$

$$\gamma_{nz} = \gamma_{xz}^\circ \sin\theta - \gamma_{yz}^\circ \cos\theta - \gamma_\omega^\circ q \tag{16c}$$

III. VARIATIONAL FORMULATION

The total potential energy of the system can be stated, in its buckled shape, as

$$\Pi = \mathcal{U} + \mathcal{V} \tag{17}$$

where $\mathcal{U}$ is the strain energy

$$\mathcal{U} = \frac{1}{2}\int_v (\sigma_z\epsilon_z + \sigma_{sz}\gamma_{sz} + \sigma_{nz}\gamma_{sz})dv \tag{18}$$

After substituting Eq.(16) into Eq.(18)

$$\begin{aligned}\mathcal{U} = \frac{1}{2}\int_v \Big\{ & \sigma_z\Big[\epsilon_z^\circ + (x + n\sin\theta)\kappa_y + (y - n\cos\theta)\kappa_x + (\omega - nq)\kappa_\omega\Big] \\ & + \sigma_{sz}\Big[\gamma_{xz}^\circ\cos\theta + \gamma_{yz}^\circ\sin\theta + \gamma_\omega^\circ r + n\kappa_{sz}\Big] + \sigma_{nz}\Big[\gamma_{xz}^\circ\sin\theta - \gamma_{yz}^\circ\cos\theta + \gamma_\omega^\circ q\Big]\Big\}dv\end{aligned} \tag{19}$$

The variation of strain energy, Eq.(19), can be stated as

$$\delta\mathcal{U} = \int_0^l (N_z\delta\epsilon_z + M_y\delta\kappa_y + M_x\delta\kappa_x + M_\omega\delta\kappa_\omega + V_x\delta\gamma_{xz}^\circ + V_y\delta\gamma_{yz}^\circ + T\delta\gamma_\omega^\circ + M_t\delta\kappa_{sz})ds \tag{20}$$

where $N_z, M_x, M_y, M_\omega, V_x, V_y, T, M_t$ are axial force, bending moments in the x- and y-directions, warping moment (bimoment), and torsional moment with respect to the centroid, respectively, defined by integrating over the

cross-sectional area A as

$$N_z = \int_A \sigma_z ds dn \tag{21a}$$

$$M_y = \int_A \sigma_z (x + n\sin\theta) ds dn \tag{21b}$$

$$M_x = \int_A \sigma_z (y - n\cos\theta) ds dn \tag{21c}$$

$$M_\omega = \int_A \sigma_z (\omega - nq) ds dn \tag{21d}$$

$$V_x = \int_A (\sigma_{sz}\cos\theta + \sigma_{nz}\sin\theta) ds dn \tag{21e}$$

$$V_y = \int_A (\sigma_{sz}\sin\theta - \sigma_{nz}\cos\theta) ds dn \tag{21f}$$

$$T = \int_A (\sigma_{sz} r + \sigma_{nz} q) ds dn \tag{21g}$$

$$M_t = \int_A \sigma_{sz} n ds dn \tag{21h}$$

The potential of in-plane loads $\mathcal{V}$ due to transverse deflection

$$\mathcal{V} = \frac{1}{2}\int_v \overline{\sigma}_z^0 \Big[(u')^2 + (v')^2\Big] dv \tag{22}$$

where $\overline{\sigma}_z^0$ is the averaged constant in-plane edge axial stress, defined by $\overline{\sigma}_z^0 = P^0/A$. The variation of the potential of in-plane loads at the centroid is expressed by substituting the assumed displacement field into Eq.(22) as

$$\begin{aligned}\delta\mathcal{V} = \int_v \frac{P^0}{A}\Big[&U'\delta U' + V'\delta V' + (q^2 + r^2 + 2rn + n^2)\Phi'\delta\Phi' + (\Phi'\delta U' + U'\delta\Phi')\big[n\cos\theta - (y - y_p)\big] \\ &+ (\Phi'\delta V' + V'\delta\Phi')\big[n\cos\theta + (x - x_p)\big]\Big] dv\end{aligned} \tag{23}$$

The kinetic energy of the system is given by

$$\mathcal{T} = \frac{1}{2}\int_v \rho(\dot{u}^2 + \dot{v}^2 + \dot{w}^2) dv \tag{24}$$

where ρ is a density.

The variation of the kinetic energy is expressed by substituting the assumed displacement field into Eq.(24) as

$$\begin{aligned}
\delta\mathcal{T} &= \int_v \rho\Big\{\delta\dot{W}\Big[\dot{W}+\dot{\Psi}_x(y-n\cos\theta)+\dot{\Psi}_y(x+n\sin\theta)+\dot{\Psi_\omega}(\omega-nq)\Big] \\
&+ \delta\dot{U}\Big[\dot{U}+\dot{\Phi}\Big[n\cos\theta-(y-y_p)\Big]\Big]+\delta\dot{V}\Big[m_0\dot{V}+\dot{\Phi}\Big[n\sin\theta+(x-x_p)\Big]\Big] \\
&+ \delta\dot{\Phi}\dot{\Phi}\Big[\dot{U}\Big[n\cos\theta-(y-y_p)\Big]+\dot{V}\Big[n\sin\theta+(x-x_p)\Big]+\dot{\Phi}(q^2+r^2+2rn+n^2)\Big] \\
&+ \delta\dot{\Psi}_x\dot{\Psi}_x\Big[\dot{W}(y-n\cos\theta)+\dot{\Psi}_x(y-n\cos\theta)^2+\dot{\Psi}_y(x+n\sin\theta)(y-n\cos\theta)+\dot{\Psi}_\omega(y-n\cos\theta)(\omega-nq)\Big] \\
&+ \delta\dot{\Psi_y}\dot{\Psi}_y\Big[\dot{W}(x+n\sin\theta)+\dot{\Psi}_x(x+n\sin\theta)(y-n\cos\theta)+\dot{\Psi}_y(x+n\sin\theta)^2+\dot{\Psi}_\omega(x+n\sin\theta)(\omega-nq)\Big] \\
&+ \delta\dot{\Psi_\omega}\dot{\Psi}_\omega\Big[\dot{W}(\omega-nq)+\dot{\Psi}_x(y-n\cos\theta)(\omega-nq)+\dot{\Psi}_y(x+n\sin\theta)(\omega-nq)+\dot{\Psi}_\omega(\omega-nq)^2\Big]\Big\}dv \qquad (25)
\end{aligned}$$

In Eqs.(23) and (25), the following geometric relations are used (Fig.1)

$$x-x_p = q\cos\theta+r\sin\theta \qquad (26a)$$

$$y-y_p = q\sin\theta-r\cos\theta \qquad (26b)$$

In order to derive the equations of motion, Hamilton's principle is used

$$\delta\int_{t_1}^{t_2}(\mathcal{T}-\Pi)dt = 0 \qquad (27)$$

Substituting Eqs.(20), (23) and (25) into Eq.(27), the following weak statement is obtained

$$\begin{aligned}
0 &= \int_{t_1}^{t_2}\int_0^l\Big\{\delta\dot{W}\Big[m_0\dot{W}-m_c\dot{\Psi}_x+m_s\dot{\Psi}_y+(m_\omega-m_q)\dot{\Psi_\omega}\Big]+\delta\dot{U}\Big[m_0\dot{U}+(m_c+y_pm_0)\dot{\Phi}\Big] \\
&+ \delta\dot{V}\Big[m_0\dot{V}+(m_s-x_pm_0)\dot{\Phi}\Big]+\delta\dot{\Phi}\Big[(m_c+y_pm_0)\dot{U}+(m_s-x_pm_0)\dot{V}+(m_p+m_2+2m_r)\dot{\Phi}\Big] \\
&+ \delta\dot{\Psi}_x\Big[-m_c\dot{W}+(m_{y2}-2m_{yc}+m_{c2})\dot{\Psi}_x+(m_{xycs}-m_{cs})\dot{\Psi}_y+(m_{y\omega}-m_{y\omega qc}+m_{qc})\dot{\Psi}_\omega\Big] \\
&+ \delta\dot{\Psi}_y\Big[m_s\dot{W}+(m_{xycs}-m_{cs})\dot{\Psi}_x+(m_{x2}+2m_{xs}+m_{s2})\dot{\Psi}_y+(m_{x\omega}+m_{x\omega qs}-m_{qs})\dot{\Psi}_\omega\Big] \\
&+ \delta\dot{\Psi_\omega}\Big[(m_\omega-m_q)\dot{W}+(m_{y\omega}-m_{y\omega qc}+m_{qc})\dot{\Psi}_x+(m_{x\omega}+m_{x\omega qs}-m_{qs})\dot{\Psi}_y+(m_{\omega 2}-2m_{q\omega}+m_{q2})\dot{\Psi}_\omega\Big] \\
&- P^0\big[\delta U'(U'+\Phi'y_p)+\delta V'(V'-\Phi'x_p)+\delta\Phi'(\Phi'\frac{I_p}{A}+U'y_p-V'x_p)\big]-N_z\delta W' \\
&- M_y\delta\Psi'_y-M_x\delta\Psi'_x-M_\omega\delta\Psi'_\omega-V_x\delta(U'+\Psi_y)-V_y\delta(V'+\Psi_x)-T\delta(\Phi'-\Psi_\omega)-M_t\delta(\Phi'-\Psi_\omega)\Big\}dzdt \qquad (28)
\end{aligned}$$

All the inertia coefficients in Eq.(28) are given in Appendix.

IV. CONSTITUTIVE EQUATIONS

The constitutive equations of a k^{th} orthotropic lamina in the laminate co-ordinate system of section are given by

$$\left\{ \begin{array}{c} \sigma_z \\ \sigma_{sz} \end{array} \right\}^k = \left[\begin{array}{cc} \bar{Q}^*_{11} & \bar{Q}^*_{16} \\ \bar{Q}^*_{16} & \bar{Q}^*_{66} \end{array} \right]^k \left\{ \begin{array}{c} \epsilon_z \\ \gamma_{sz} \end{array} \right\} \tag{29}$$

where $\bar{Q}^*_{ij}$ are transformed reduced stiffnesses. The transformed reduced stiffnesses can be calculated from the transformed stiffnesses based on the plane stress assumption and plane strain assumption. More detailed explanation can be found in Ref.[31]

The constitutive relation for out-of-plane stress and strain is given by

$$\sigma_{nz} = \bar{Q}_{55}\gamma_{nz} \tag{30}$$

The constitutive equations for bar forces and bar strains are obtained by using Eqs.(16), (21) and (29)

$$\left\{ \begin{array}{c} N_z \\ M_y \\ M_x \\ M_\omega \\ M_t \\ V_x \\ V_y \\ T \end{array} \right\} = \left[\begin{array}{cccccccc} E_{11} & E_{12} & E_{13} & E_{14} & E_{15} & E_{16} & E_{17} & E_{18} \\ & E_{22} & E_{23} & E_{24} & E_{25} & E_{26} & E_{27} & E_{28} \\ & & E_{33} & E_{34} & E_{35} & E_{36} & E_{37} & E_{38} \\ & & & E_{44} & E_{45} & E_{46} & E_{47} & E_{48} \\ & & & & E_{55} & E_{56} & E_{57} & E_{58} \\ & & & & & E_{66} & E_{67} & E_{68} \\ & & & & & & E_{77} & E_{78} \\ \text{sym.} & & & & & & & E_{88} \end{array} \right] \left\{ \begin{array}{c} \epsilon^\circ_z \\ \kappa_y \\ \kappa_x \\ \kappa_\omega \\ \kappa_{sz} \\ \gamma^\circ_{xz} \\ \gamma^\circ_{yz} \\ \gamma^\circ_\omega \end{array} \right\} \tag{31}$$

where E_{ij} are stiffnesses of thin-walled composite beams and given in Ref.[30].

V. EQUATIONS OF MOTION

The equations of motion of the present study can be obtained by integrating the derivatives of the varied quantities by parts and collecting the coefficients of $\delta W, \delta U, \delta V, \delta\Phi, \delta\Psi_y, \delta\Psi_x$ and $\delta\Psi_\omega$

$$N_z' = m_0\ddot{W} - m_c\ddot{\Psi}_x + m_s\ddot{\Psi}_y + (m_\omega - m_q)\ddot{\Psi}_\omega \tag{32a}$$

$$V_x' + P^0\big(U'' + \Phi'' y_p\big) = m_0\ddot{U} + (m_c + y_p m_0)\ddot{\Phi} \tag{32b}$$

$$V_y' + P^0\big(V'' - \Phi'' x_p\big) = m_0\ddot{V} + (m_s - x_p m_0)\ddot{\Phi} \tag{32c}$$

$$M_t' + T' + P^0\big(\Phi''\frac{I_p}{A} + U'' y_p - V'' x_p\big) = (m_c - m_y + y_p m_0)\ddot{U} + (m_s - x_p m_0)\ddot{V} + (m_p + m_2 + 2m_r)\ddot{\Phi} \tag{32d}$$

$$M_y' - V_x = m_s\ddot{W} + (m_{xycs} - m_{cs})\ddot{\Psi}_x + (m_{x2} + 2m_{xs} + m_{s2})\ddot{\Psi}_y \tag{32e}$$

$$+ (m_{x\omega} + m_{x\omega qs} - m_{qs})\ddot{\Psi}_\omega \tag{32f}$$

$$M_x' - V_y = -m_c\ddot{W} + (m_{y2} - 2m_{yc} + m_{c2})\ddot{\Psi}_x + (m_{xycs} - m_{cs})\ddot{\Psi}_y \tag{32g}$$

$$+ (m_{y\omega} - m_{y\omega qc} + m_{qc})\ddot{\Psi}_\omega \tag{32h}$$

$$M_\omega' + M_t - T = (m_\omega - m_q)\ddot{W} + (m_{y\omega} - m_{y\omega qc} + m_{qc})\ddot{\Psi}_x \tag{32i}$$

$$+ (m_{x\omega} + m_{x\omega qs} - m_{qs})\ddot{\Psi}_y$$

$$+ (m_{\omega 2} - 2m_{q\omega} + m_{q2})\ddot{\Psi}_\omega \tag{32j}$$

The natural boundary conditions are of the form

$$\delta W \ : \ N_z \tag{33a}$$

$$\delta U \ : \ V_x \tag{33b}$$

$$\delta V \ : \ V_y \tag{33c}$$

$$\delta\Phi \ : \ T + M_t \tag{33d}$$

$$\delta\Psi_y \ : \ M_y \tag{33e}$$

$$\delta\Psi_x \ : \ M_x \tag{33f}$$

$$\delta\Psi_\omega \ : \ M_\omega \tag{33g}$$

The 7^{th} denotes the warping restraint boundary condition. When the warping of the cross section is restrained, $\Psi_\omega = 0$ and when the warping is not restrained, $M_\omega = 0$.

Eq.(32) is most general form for axial-flexural-torsional-shearing vibration of thin-walled composite beams. For general anisotropic materials, the dependent variables, U, V, W, Φ, Ψ_x, Ψ_y and Ψ_ω are fully-coupled implying that

the beam undergoes a coupled behavior involving bending, twising, extension, transverse shearing, and warping. The resulting coupling is referred to as sixfold coupled vibrations. If all the coupling effects and axial force are neglected as well as cross section is symmetrical with respect to both x- and the y-axes, Eq.(32) can be simplified to the uncoupled differential equations as

$$(EA)_{com}W'' = \rho A\ddot{W} \tag{34a}$$

$$(GA_y)_{com}(U'' + \Psi_y') = \rho A\ddot{U} \tag{34b}$$

$$(GA_x)_{com}(V'' + \Psi_x') = \rho A\ddot{V} \tag{34c}$$

$$(GJ_1)_{com}\Phi'' - (GJ_2)_{com}\Psi_\omega' = \rho I_p\ddot{\Phi} \tag{34d}$$

$$(EI_y)_{com}\Psi_y'' - (GA_y)_{com}(U' + \Psi_y) = \rho I_y\ddot{\Psi}_y \tag{34e}$$

$$(EI_x)_{com}\Psi_x'' - (GA_x)_{com}(V' + \Psi_x) = \rho I_x\ddot{\Psi}_x \tag{34f}$$

$$(EI_\omega)_{com}\Psi_\omega'' + (GJ_2)_{com}\Phi' - (GJ_1)_{com}\Psi_\omega = \rho I_\omega\ddot{\Psi}_\omega \tag{34g}$$

From above equations, $(EA)_{com}$ represents axial rigidity, $(GA_x)_{com}$, $(GA_y)_{com}$ represent shear rigidities with respect to x- and y-axis, $(EI_x)_{com}$ and $(EI_y)_{com}$ represent flexural rigidities with respect to x- and y-axis, $(EI_\omega)_{com}$ represents warping rigidity, and $(GJ)_{com}$, $(GJ_1)_{com}$, $(GJ_2)_{com}$ represent torsional rigidities of the thin-walled composite beams, respectively, written as

$$(EA)_{com} = E_{11} \tag{35a}$$

$$(EI_y)_{com} = E_{22} \tag{35b}$$

$$(EI_x)_{com} = E_{33} \tag{35c}$$

$$(EI_\omega)_{com} = E_{44} \tag{35d}$$

$$(GJ)_{com} = 4E_{55} \tag{35e}$$

$$(GA_y)_{com} = E_{66} \tag{35f}$$

$$(GA_x)_{com} = E_{77} \tag{35g}$$

$$(GA_\omega)_{com} = E_{88} \tag{35h}$$

$$(GJ_1)_{com} = E_{55} + E_{88} \tag{35i}$$

$$(GJ_2)_{com} = E_{55} - E_{88} \tag{35j}$$

In Eq.(34), I_p denotes the polar moment of inertia. It is well known that the three distinct vibration modes flexural

vibration in the x- and y-direction and torsional vibration, are identified in this case and the corresponding natural frequencies are given by the approximate solution or orthotropy solution for a clamped beam boundary conditions [11]

$$\omega_{x_n} = \sqrt{\Big[\frac{\rho A}{(EI_y)_{com}}\frac{L^4}{(n+0.5)^4\pi^4} + \frac{\rho A}{(GA_y)_{com}}\frac{L^2}{n^2\pi^2}\Big]^{-1}} \tag{36a}$$

$$\omega_{y_n} = \sqrt{\Big[\frac{\rho A}{(EI_x)_{com}}\frac{L^4}{(n+0.5)^4\pi^4} + \frac{\rho A}{(GA_x)_{com}}\frac{L^2}{n^2\pi^2}\Big]^{-1}} \tag{36b}$$

$$\omega_{\theta_n} = \sqrt{\Big[\frac{\rho I_p}{(EI_\omega)_{com}}\frac{L^4}{(n+0.5)^4\pi^4} + \frac{\rho I_p}{(GA_\omega)_{com}}\frac{L^2}{n^2\pi^2}\Big]^{-1} + \frac{(GJ)_{com}}{\rho I_p}\frac{n^2\pi^2}{L^2}} \tag{36c}$$

where $\omega_{x_n}, \omega_{y_n}, \omega_{\theta_n}$ are the flexural natural frequencies in the x- and y-direction, and torsional natural frequency, respectively.

VI. FINITE ELEMENT FORMULATION

The present theory for thin-walled composite beams described in the previous section was implemented via a displacement based one-dimensional finite element method. The generalized displacements are expressed over each element as a combination of the one-dimensional Lagrange interpolation function ψ_j associated with node j and the nodal values

$$W = \sum_{j=1}^{n} w_j\psi_j \tag{37a}$$

$$U = \sum_{j=1}^{n} u_j\psi_j \tag{37b}$$

$$V = \sum_{j=1}^{n} v_j\psi_j \tag{37c}$$

$$\Phi = \sum_{j=1}^{n} \phi_j\psi_j \tag{37d}$$

$$\Psi_y = \sum_{j=1}^{n} \psi_{yj}\psi_j \tag{37e}$$

$$\Psi_x = \sum_{j=1}^{n} \psi_{xj}\psi_j \tag{37f}$$

$$\Psi_\omega = \sum_{j=1}^{n} \psi_{\omega j}\psi_j \tag{37g}$$

Substituting these expressions into the weak statement in Eq.(28), the finite element model of a typical element can be expressed as

$$([K] - P^0[G] - \omega^2[M])\{\Delta\} = \{0\} \tag{38}$$

where $[K], [G]$ and $[M]$ are the element stiffness matrix, the element geometric stiffness matrix and the element mass matrix, respectively. More detailed explanation explicit forms of $[K]$ can be found in Ref.[30] and those of $[G]$ and $[M]$ are given in Appendix.

In Eq.(38), $\{\Delta\}$ is the eigenvector of nodal displacements corresponding to an eigenvalue

$$\{\Delta\} = \{W\ U\ V\ \Phi\ \Psi_y\ \Psi_x\ \Psi_\omega\}^{\mathrm{T}} \tag{39}$$

VII. NUMERICAL EXAMPLES

For verification purpose, the buckling behavior and free vibration of a cantilever isotropic mono-symmetric channel section beam, as shown in Fig.2, with length l =200cm under axial force at the centroid is performed. The material properties are assumed to be: $E = 3 \times 10^4\mathrm{N/cm}^2$, $G = 1.15 \times 10^4\mathrm{N/cm}^2$, $\rho = 7.85 \times 10^{-3}\mathrm{N/cm}^3$. The buckling loads and natural frequencies are evaluated and compared with numerical results of Kim et al.[32] which is based on dynamic stiffness formulation and ABAQUS solutions in Table I. The present results are in a good agreement with those by Kim et al.[32].

The next example demonstrates the accuracy and validity of this study for thin-walled composite beams. Ten quadratic elements with three nodes are used in the numerical computation. The symmetric angle-ply I-beams with various fiber angles and boundary conditions are considered. Following dimensions for I-beam are used: both of flanges width and web height are 5cm. The flanges and web are assumed to be symmetrically laminated with respect to its midplane and made of sixteen layers with each layer 0.013cm in thickness. All computations are carried out for the glass-epoxy materials with the following material properties: $E_1 = 53.78\mathrm{GPa}$, $E_2 = 17.93\mathrm{GPa}$, $G_{12} = G_{13} = 8.96\mathrm{GPa}$, $G_{23} = 3.45\mathrm{GPa}$, $\nu_{12} = 0.25$. The critical buckling loads for a cantilever composite beam with length l =100cm and the natural frequencies for a simply supported one with length l =200cm under compressive force at the centroid are presented. The comparison of the results obtained from the proposed finite element solution, the analytical approach by Kim et al.[25,26] are given in Tables II and III for different stacking sequences. The present solution again indicates good agreement with the analytical solution and ABAQUS results for all lamination schemes considered. The effect of compressive axial force on the fundamental natural frequencies of the cantilever and simply supported beam with various fiber angles is exhibited in Figs.3 and 4. It can be seen that the change in the natural

frequency due to axial force is noticeable. The natural frequency diminishes when the axial force changes from tensile to compressive, as expected. It is obvious that the natural frequency decreases with the increase of axial force, and the decrease becomes more quickly when the fiber angle increases and the axial force is close to critical buckling load. With $\theta = 0°$, $30°$ and $60°$, at about P=5.74×10^3N, 3.85×10^3N and 2.11×10^3N, respectively, for simply supported beam, the natural frequencies become zero which implies that at these loads, flexural-torsional bucklings occur as a degenerate case of natural vibration at zero frequency. Moreover, Figs.3 and 4 also explain the duality between flexural-torsional buckling and natural frequency.

In order to investigate the coupling and shear effects on the natural frequencies and mode shapes, a clamped thin-walled composite I-beam is considered. The geometry of the I-section is shown in Fig.5, and the following engineering constants are used

$$E_1/E_2 = 25, G_{12}/E_2 = 0.6, G_{13} = G_{12} = G_{23}, \nu_{12} = 0.25 \tag{40}$$

For convenience, the following nondimensional natural frequency is used

$$\bar{\omega} = \frac{\omega l^2}{b_3}\sqrt{\frac{\rho}{E_2}} \tag{41}$$

The top and bottom flanges are considered as angle-ply laminates $[\theta/-\theta]$ and the web laminates are assumed to be unidirectional, (Fig.5a). For this lay-up, the coupling stiffnesses E_{35}, E_{38} do not vanish due to unsymmetric stacking sequence of the flanges. The lowest three natural frequencies by model of no shear effects based on previous research [28] and the present model with $l/b_3 = 20$ are given in Table.IV. It is interesting to note that as fiber angle increases, the shear effects decrease and become negligbly small especially in the interval $\theta \in [30°, 90°]$ even for the lower span-to-height ratio and higher natural frequencies. This trend can be explained that flexural stiffnesses decrease significantly with increasing fiber angle, and thus, the relative shear effects become smaller for higher fiber angles. The lowest three natural frequencies by the finite element analysis and the orthotropy solutions, which neglects the coupling effects of E_{35}, E_{38}, from Eqs.(36a)-(36c) for each mode are illustrated in Fig.6. Due to coupling stiffnesses, the orthotropy solution might not be accurate. However, as fiber angle increases, the coupling effects coming from the material anisotropy become negligible. Therefore, it can be seen in Fig.6, for all cases of fiber angle, the lowest two natural frequencies by the finite element analysis always correspond to the first flexural mode in x-direction and the torsional mode. Vice versa, the third mode exhibits the first flexural mode in y-direction in the range of $\theta \in [0°, 25°]$, and after this range, this mode becomes predominantly the second flexural mode in x-direction. It can be explained partly by the mode shapes corresponding to ω_1, ω_2 and ω_3 with fiber angle $\theta = 30°$ in Figs.7-9. In each

mode the amplitude along the beam length is nomalized with respect to the maximum amplitude for that mode. Since the vibration mode 1, 2 and 3 are purely first flexural x-direction, torsional mode and the second flexural mode in x-direction, the othotropy solution and the finite element analysis are identical. It is indicated that the simple orthotropy solution is sufficiently accurate for this lay-up.

To investigate the coupling and shear effects further, the same configuration with the previous example except the laminate stacking sequence is considered. Stacking sequence of the top flange and web are considered as $[0/45^\circ]$, while the bottom flange is $[\theta_2]$, (Fig.5b). All the coupling stiffnesses, especially, $E_{16}, E_{17}, E_{18}, E_{36}, E_{38}$ and E_{78} become no more negligibly small. Table.V shows that the solutions excluding shear effects remarkably underestimate the natural frequencies for all the range of fiber angle even for higher span-to-height ratio. It is indicated that the coupling effects become significant because the transverse shear little affects the behavior of this beam ($l/b_3 = 50$). This implies that discarding shear effects leads to an overprediction of the natural frequencies especially for higher modes. Thus, the orthotropy solution and the finite element solution show discrepancy in Fig.10. The mode shapes corresponding to the lowest three natural frequencies with fiber angle $\theta = 30^\circ$ are illustrated in Figs.11-13. Relative measures of flexural displacements, torsional and shearing rotation show that when the beam is vibrating at the natural frequency belonging to the first and second mode exhibits fourfold coupled mode (flexural vibration in the x-direction, torsional and corresponding shearing vibration), whereas, third mode displays sixfold coupled mode (flexural mode in the x-, y-direction, torsional mode and corresponding shearing vibration). This fact explains as the fiber angle changes, for lower span-to-height ratio (Fig.10), the orthotropy solutions disagree with the finite element solutions as anisotropy of the beam gets higher. That is, the orthotropy solution is no longer valid for unsymmetrically laminated beams, and sixfold coupled flexural-torsional-shearing vibration should be considered even for a doubly symmetric cross-section.

VIII. CONCLUDING REMARKS

An analytical model based on shear-deformable beam theory is developed to study the flexural-torsional coupled vibration and buckling of thin-walled composite beams. This model is capable of predicting accurate natural frequencies, buckling loads as well as corresponding mode shapes for various configuration including boundary conditions, laminate orientation and span-to-height ratio. To formulate the problem, a one-dimensional displacement-based finite element method is employed. All of the possible vibration modes including the flexural mode in the x- and y-direction, the torsional mode, and fully coupled flexural-torsional-shearing mode are included in the analysis. The shear effects become significant for lower span-to-height ratio and higher degrees of orthotropy of the beam. The orthotropy solu-

tion is accurate for lower degrees of material anisotropy, but, becomes inappropriate as the anisotropy of the beam gets higher, and fully coupled equations should be considered for accurate analysis of thin-walled composite beams. The present model is found to be appropriate and efficient in analyzing flexural-torsional coupled vibration and buckling of thin-walled composite beams.

Acknowledgments

The support of the research reported here by Seoul R&BD Program through Grant GR070033 is gratefully acknowledged. The authors also would like to thank the anonymous reviewers for their suggestions in improving the standard of the manuscript.

APPENDIX

Inertia coefficients in Eq.(28) are defined by

$$m_0 = I_0 \int_s ds \tag{42a}$$

$$m_c = I_1 \int_s \cos\theta ds \tag{42b}$$

$$m_r = I_1 \int_s r ds \tag{42c}$$

$$m_p = I_0 \int_s (q^2 + r^2) ds \tag{42d}$$

$$m_q = I_1 \int_s q ds \tag{42e}$$

$$m_s = I_1 \int_s \sin\theta ds \tag{42f}$$

$$m_\omega = I_0 \int_s \omega ds \tag{42g}$$

$$m_2 = I_2 \int_s ds \tag{42h}$$

$$m_{c2} = I_2 \int_s \cos^2\theta ds \tag{42i}$$

$$m_{s2} = I_2 \int_s \sin^2\theta ds \tag{42j}$$

$$m_{q2} = I_2 \int_s q^2 ds \tag{42k}$$

$$m_{x2} = I_0 \int_s x^2 ds \tag{42l}$$

$$m_{y2} = I_0 \int_s y^2 ds \tag{42m}$$

$$m_{\omega 2} = I_0 \int_s \omega^2 ds \tag{42n}$$

$$m_{cs} = I_2 \int_s \sin\theta\cos\theta ds \tag{42o}$$

$$m_{qc} = I_2 \int_s q \cos\theta ds \tag{42p}$$

$$m_{qs} = I_2 \int_s q \sin\theta ds \tag{42q}$$

$$m_{xs} = I_1 \int_s x \sin\theta ds \tag{42r}$$

$$m_{yc} = I_1 \int_s y \cos\theta ds \tag{42s}$$

$$m_{q\omega} = I_1 \int_s q\omega ds \tag{42t}$$

$$m_{x\omega} = I_0 \int_s x\omega ds \tag{42u}$$

$$m_{y\omega} = I_0 \int_s y\omega ds \tag{42v}$$

$$m_{\omega c} = I_1 \int_s \omega \cos\theta ds \tag{42w}$$

$$m_{\omega s} = I_1 \int_s \omega \sin\theta ds \tag{42x}$$

$$m_{xycs} = I_1 \int_s (-x\cos\theta + y\sin\theta) ds \tag{42y}$$

$$m_{x\omega qs} = I_1 \int_s (-qx + \omega\sin\theta) ds \tag{42z}$$

$$m_{y\omega qc} = I_1 \int_s (qy + \omega\cos\theta) ds \tag{42aa}$$

where

$$(I_0, I_1, I_2) = \int_n \rho(1, n, n^2) dn \tag{43}$$

$[M]$ is the 7×7 element mass matrix with coefficients given by

$$M_{ij}^{11} = M_{ij}^{22} = M_{ij}^{33} = \int_0^l m_0 \psi_i \psi_j dz \tag{44a}$$

$$M_{ij}^{15} = \int_0^l m_s \psi_i \psi_j dz \tag{44b}$$

$$M_{ij}^{16} = -\int_0^l m_c \psi_i \psi_j dz \tag{44c}$$

$$M_{ij}^{17} = \int_0^l (m_\omega - m_q) \psi_i \psi_j dz \tag{44d}$$

$$M_{ij}^{24} = \int_0^l (m_c + m_0 y_p) \psi_i \psi_j dz \tag{44e}$$

$$M_{ij}^{34} = \int_0^l (m_s - m_0 x_p) \psi_i \psi_j dz \tag{44f}$$

$$M_{ij}^{44} = \int_0^l (m_p + m_2 + 2m_r) \psi_i \psi_j dz \tag{44g}$$

$$M_{ij}^{55} = \int_0^l (m_{x2} + 2m_{xs} + m_{s2}) \psi_i \psi_j dz \tag{44h}$$

$$M_{ij}^{56} = \int_0^l (m_{xycs} - m_{cs})\psi_i\psi_j dz \tag{44i}$$

$$M_{ij}^{57} = \int_0^l (m_{x\omega} + m_{x\omega qs} - m_{qs})\psi_i\psi_j dz \tag{44j}$$

$$M_{ij}^{66} = \int_0^l (m_{y2} - 2m_{yc} + m_{c2})\psi_i\psi_j dz \tag{44k}$$

$$M_{ij}^{67} = \int_0^l (m_{y\omega} - m_{y\omega qc} + m_{qc})\psi_i\psi_j dz \tag{44l}$$

$$M_{ij}^{77} = \int_0^l (m_{\omega 2} - 2m_{q\omega} + m_{q2})\psi_i\psi_j dz \tag{44m}$$

and $[G]$ is the 7×7 element geometric stiffness matrix with coefficients given by

$$G_{ij}^{22} = G_{ij}^{33} = \int_0^l \psi_i'\psi_j' dz \tag{45a}$$

$$G_{ij}^{24} = \int_0^l y_p\psi_i'\psi_j' dz \tag{45b}$$

$$G_{ij}^{34} = -\int_0^l x_p\psi_i'\psi_j' dz \tag{45c}$$

$$G_{ij}^{44} = \int_0^l \frac{I_p}{A}\psi_i'\psi_j' dz \tag{45d}$$

All other components are zero.

References

[1] Vlasov VZ. Thin Walled Elastic Beams, Israel Program for Scientific Translation, Jerusalem, 1961.

[2] Gjelsvik A. The theory of thin-walled bars, New York: John Wiley and Sons Inc., 1981.

[3] Timoshenko SP and Gere JM. Theory of elastic stability. New York: McGraw-Hill, 1963.

[4] Timoshenko SP, Young DH and Weaver W. Vibration problems in engineering. New York: Wiley, 1974.

[5] Trahair NS. Flexural-torsional buckling of structures. London: CRC Press, 1993.

[6] Chandra R and Chopra I. Experimental-theoretical investigation of the vibration characteristics of rotating composite I-beams. J Aircraft 1992; 29(4):657-664.

[7] Song 0 and Librescu L. Dynamic Theory of Open Cross Section Thin-Walled Beams Composed of Advanced Composite Materials. J Thermoplas Compos 1995; 8(2):225-238.

[8] Librescu L and Song 0. Thin-walled Composite Beams. Springer, 2006.

[9] Kollar LP. Flexural-torsional buckling of open section composite columns with shear deformation. Int J Solids Struct 2001; 38(42-43):7525-7541.

[10] Kollar LP. Flexural-torsional vibration of open section composite columns with shear deformation. Int J Solids Struct 2001; 38(42-43):7543-7558.

[11] Kollar LP and Springer GS. Mechanics of composite structure. Cambridge University Press, 2003.

[12] Qiao P and Zou G. Free Vibration Analysis of Fiber-Reinforced Plastic Composite Cantilever I-Beams. Mech Adv Mater Struct 2002; 9(4):7359-373.

[13] Della CN and Shu DW. Vibration of Beams with Two Overlapping Delaminations in Prebuckled States. Compos part B 2007; 38:109-118.

[14] Della CN and Shu DW. Vibration of Delaminated Composite Laminates: A Review. ASME Appl Mech Rev 2007; 60(1):1-20.

[15] Banerjee JR and Williams FW. Exact dynamic stiffness matrix for composite Timoshenko beams with applications. J Sound Vib 1996; 194(4):573-585.

[16] Banerjee JR. Free vibration of axially loaded composite Timoshenko beams using the dynamic stiffness matrix method. Comput Struct 1998;69(2):197-208.

[17] Li J, Shen R and Jin X. Bending-torsional coupled dynamic response of axially loaded composite Timosenko thin-walled beam with closed cross-section. Compos Struct 2004;64(1):23-35.

[18] Li J, Wu G, Shen R and Hua H. Stochastic bending-torsion coupled response of axially loaded slender composite thin-walled beams with closed cross-sections. Int J Mech Sci 2005; 47(1):134-155.

[19] Li J and Jin X. Response of flexure-torsion coupled composite thin-walled beams with closed cross-sections to random loads. Mech Res Commun 2005; 32(1):25-41.

[20] Bank LC and Kao CH. Dynamic Response of Thin-Walled Composite Material Timoshenko Beams. J Energ Resour 1990; 112:149-154.

[21] Cortinez VH and Piovan MT. Vibration and buckling of composite thin-walled beams with shear deformability. J Sound Vib 2002; 258(4-5):701-723.

[22] Piovan MT and Cortinez VH. Mechanics of shear deformable thin-walled beams made of composite materials. Thin-Walled Struct 2007; 45(1):37-62

[23] Machado SP, Filipich CP and Cortinez VH. Parametric vibration of thin-walled composite beams with shear deformation. J Sound Vib 2007; 305(4-5):563-581.

[24] Kim NI, Shin DK and Kim MY. Improved flexural-torsional stability analysis of thin-walled composite beam and exact stiffness matrix. Int J Mech Sci 2007; 49(8):950-969.

[25] Kim NI, Shin DK and Kim MY. Flexural-torsional buckling loads for spatially coupled stability analysis of thin-walled composite columns. Adv Eng Softw 2008; 39(12):949-961.

[26] Kim NI, Shin DK and Park YS. Dynamic stiffness matrix of thin-walled composite I-beam with symmetric and arbitrary laminations. J Sound Vib 2008; 318(1-2):364-388.

[27] Lee J and Kim S. Flexural-torsional buckling of thin-walled I-section composites. Comput Struct 2001;79(10):987-995.

[28] Lee J and Kim S. Free vibration of thin-walled composite beams with I-shaped cross-sections. Compos Struct 2002; 55(2):205-215.

[29] Lee J and Kim S. Flexural-torsional coupled vibration of thin-walled composite beams with channel sections. Comput Struct 2002; 80(2):133-144.

[30] Lee J. Flexural analysis of thin-walled composite beams using shear-deformable beam theory. Compos Struct 2005; 70(2):212-222.

[31] Jones RM. Mechanics of composite materials. New York: Hemisphere Publishing Corp., 1975.

[32] Kim MY, Kim NI and Yun HT. Exact dynamic and static stiffness matrices of shear deformable thin-walled beam-columns. J Sound Vib 2003; 267(1):29-55.

CAPTIONS OF TABLES

Table I: The bucking loads and natural frequencies a cantilever isotropic mono-symmetric channel section beam.

Table II: Critical bucking loads of a cantilever composite I-beam (N).

Table III: Natural frequencies of a simply supported composite I-beam (Hz).

Table IV: Nondimensional natural frequencies respect to the fiber angle change in top and bottom flanges of a clamped composite beam with span-to-height ratio $l/b_3 = 20$.

Table V: Nondimensional natural frequencies respect to the fiber angle change in the bottom flange of a clamped composite beam with two span-to-height ratios $l/b_3 = 10$ and 50.

CAPTIONS OF FIGURES

Figure 1: Definition of coordinates in thin-walled open sections.

Figure 2: Isotropic mono-symmetric channel section for verification.

Figure 3: The interaction diagram between critical buckling load and fundamental natural frequency of a simply supported composite beam with the fiber angle 0°, 30° and 60° in the flanges and web.

Figure 4: The interaction diagram between critical buckling load and fundamental natural frequency of a cantilever composite beam with the fiber angle 0°, 30° and 60° in the flanges and web.

Figure 5: Geometry and stacking sequences of thin-walled composite I-beam.

Figure 6: Variation of the lowest three nondimensional natural frequencies with respect to fiber angle change in the flanges of a clamped composite beam with $l/b_3 = 20$.

Figure 7: Mode shapes of the flexural and corresponding shearing components for the first mode $\omega_1 = 8.471$ of a clamped composite beam with the fiber angle 30° in the flanges with $l/b_3 = 20$.

Figure 8: Mode shapes of the torsional and corresponding shearing components for the second mode $\omega_2 = 10.092$ of a clamped composite beam with the fiber angle 30° in the flanges with $l/b_3 = 20$.

Figure 9: Mode shapes of the flexural and corresponding shearing components for the third mode $\omega_3 = 23.209$ of a clamped composite beam with the fiber angle 30° in the flanges with $l/b_3 = 20$.

Figure 10: Variation of the lowest three nondimensional natural frequencies with respect to fiber angle change in the bottom flange of a clamped composite beam with $l/b_3 = 10$.

Figure 11: Mode shapes of the flexural, torsional and corresponding shearing components for the first mode $\omega_1 = 8.678$ of a clamped composite beam with the fiber angle 30° in the bottom flange with $l/b_3 = 10$.

Figure 12: Mode shapes of the flexural, torsional and corresponding shearing components for the second mode $\omega_2 = 11.966$ of a clamped composite beam with the fiber angle 30° in the bottom flange with $l/b_3 = 10$.

Figure 13: Mode shapes of the flexural, torsional and corresponding shearing components for the third mode $\omega_3 = 18.980$ of a clamped composite beam with the fiber angle 30° in the bottom flange with $l/b_3 = 10$.

TABLE I The bucking loads and natural frequencies a cantilever isotropic mono-symmetric channel section beam.

Mode	Buckling loads (N)			Natural frequencies $(rad/s)^2$		
	Ref.[32]			Ref.[32]		
	ABAQUS	Theory	Present	ABAQUS	Theory	Present
1	0.027	0.028	0.026	13.789	14.001	12.977
2	0.334	0.331	0.334	111.840	113.100	113.440
3	0.704	0.696	0.707	191.160	190.080	190.567
4	1.065	1.074	1.084	255.100	256.670	263.999

TABLE II Critical bucking loads of a cantilever composite I-beam (N).

Lay-ups	Ref.[25]		Present
	ABAQUS	Theory	
$[0]_{16}$	5720.0	5755.2	5741.5
$[15/-15]_{4s}$	5174.0	5199.8	5189.0
$[30/-30]_{4s}$	3848.0	3861.0	3854.5
$[45/-45]_{4s}$	2665.0	2672.7	2668.4
$[60/-60]_{4s}$	2119.0	2114.7	2111.3
$[75/-75]_{4s}$	1950.0	1948.3	1945.1
$[0/90]_{4s}$	3848.0	3857.8	3829.8

TABLE III Natural frequencies of a simply supported composite I-beam (Hz).

Lay-ups	Formulation	Mode					
		1	2	3	4	5	6
$[0]_{16}$	Ref.[26]	24.194	35.233	45.235	96.726	109.441	180.616
	Present	24.150	35.169	45.063	96.392	109.011	178.129
$[15/-15]_{4s}$	Ref.[26]	22.997	36.247	42.996	91.940	107.655	171.678
	Present	22.955	36.067	42.851	91.701	107.156	169.616
$[30/-30]_{4s}$	Ref.[26]	19.816	37.051	37.864	79.225	102.159	147.938
	Present	19.776	36.797	36.953	79.133	100.473	146.658
$[45/-45]_{4s}$	Ref.[26]	16.487	30.827	37.915	65.916	94.884	123.085
	Present	16.446	30.758	35.125	65.895	90.447	122.286
$[60/-60]_{4s}$	Ref.[26]	14.666	27.420	35.372	58.633	87.051	109.484
	Present	14.627	27.361	32.213	58.623	81.972	108.800
$[75/-75]_{4s}$	Ref.[26]	14.077	26.319	31.313	56.278	79.330	105.087
	Present	14.042	26.258	29.945	56.255	77.149	104.342
$[0/90]_{4s}$	Ref.[26]	13.970	26.119	29.175	55.850	75.767	104.287
	Present	13.937	26.056	29.133	55.820	75.652	103.494

TABLE IV Nondimensional natural frequencies respect to the fiber angle change in top and bottom flanges of a clamped composite beam with span-to-height ratio $l/b_3 = 20$.

Fiber	No shear ([28])					Present				
angle	w_1	w_2	w_3	w_4	w_5	w_1	w_2	w_3	w_4	w_5
0	16.289	18.362	44.903	47.279	50.406	15.460	17.211	33.996	40.271	44.134
15	14.401	16.429	39.698	42.154	45.561	14.122	16.064	32.174	38.063	42.818
30	8.525	10.172	23.499	26.604	31.022	8.471	10.092	23.209	25.126	27.457
45	4.880	6.228	13.452	16.021	24.622	4.862	6.202	13.392	15.919	21.991
60	3.691	4.854	10.175	12.342	19.946	3.678	4.836	10.147	12.286	19.855
75	3.386	4.438	9.334	11.294	18.298	3.374	4.421	9.308	11.239	18.211
90	3.330	4.346	9.180	11.079	17.996	3.319	4.330	9.152	11.022	17.905

TABLE V Nondimensional natural frequencies respect to the fiber angle change in the bottom flange of a clamped composite beam with two span-to-height ratios $l/b_3 = 10$ and 50.

Ratio	Fiber	No shear ([28])					Present				
l/b_3	angle	w_1	w_2	w_3	w_4	w_5	w_1	w_2	w_3	w_4	w_5
	0	13.805	15.314	38.024	39.102	42.158	11.627	14.296	22.508	29.202	33.345
	15	13.133	14.678	36.189	37.278	40.342	11.588	13.995	20.624	29.246	34.644
	30	9.571	11.574	26.302	30.360	31.804	8.678	11.966	18.980	23.249	30.062
10	45	5.467	10.197	14.908	25.900	28.077	5.115	11.873	13.712	18.565	26.182
	60	4.082	9.923	11.072	21.552	24.702	3.897	10.444	11.855	18.289	19.969
	75	3.731	9.864	10.102	19.648	24.432	3.577	9.569	11.849	18.204	18.279
	90	3.666	9.853	9.924	19.300	24.384	3.516	9.402	11.847	17.951	18.185
	0	14.082	16.446	38.512	39.112	43.623	13.088	18.257	35.408	37.544	48.414
	15	13.208	16.675	36.343	37.272	43.126	12.872	17.229	31.024	35.165	44.903
	30	10.146	13.706	27.500	30.358	34.547	9.643	15.021	25.697	26.624	38.358
50	45	7.357	10.970	18.060	25.900	28.960	6.672	14.335	16.734	24.742	30.961
	60	6.185	10.435	14.532	24.702	25.730	5.655	13.651	14.076	24.161	24.621
	75	5.837	10.310	13.564	23.839	24.432	5.358	12.792	13.971	22.899	23.975
	90	5.761	10.284	13.365	23.465	24.384	5.293	12.613	13.943	22.555	23.932

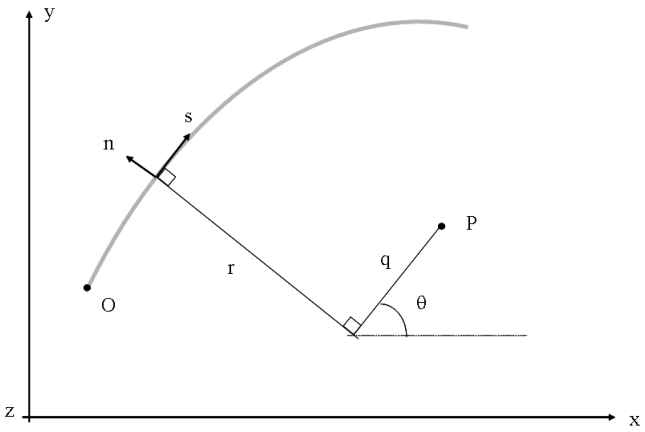

FIG. 1 Definition of coordinates in thin-walled open sections

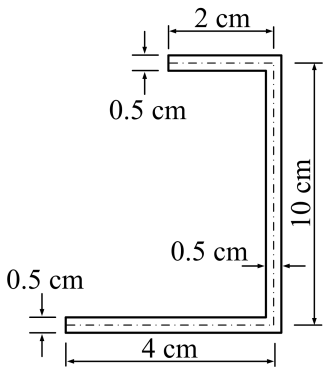

FIG. 2 Isotropic mono-symmetric channel section for verification.

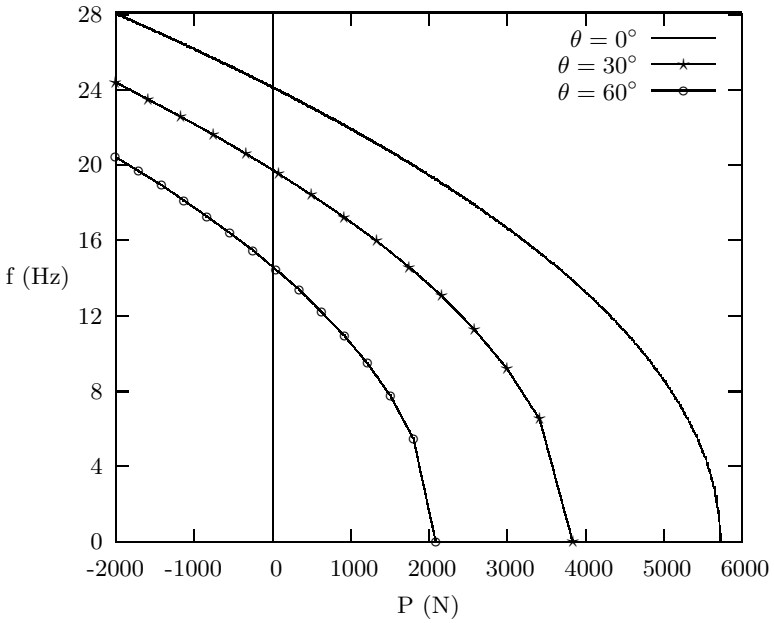

FIG. 3 The interaction diagram between critical buckling load and fundamental natural frequency of a simply supported composite beam with the fiber angle 0°, 30° and 60° in the flanges and web.

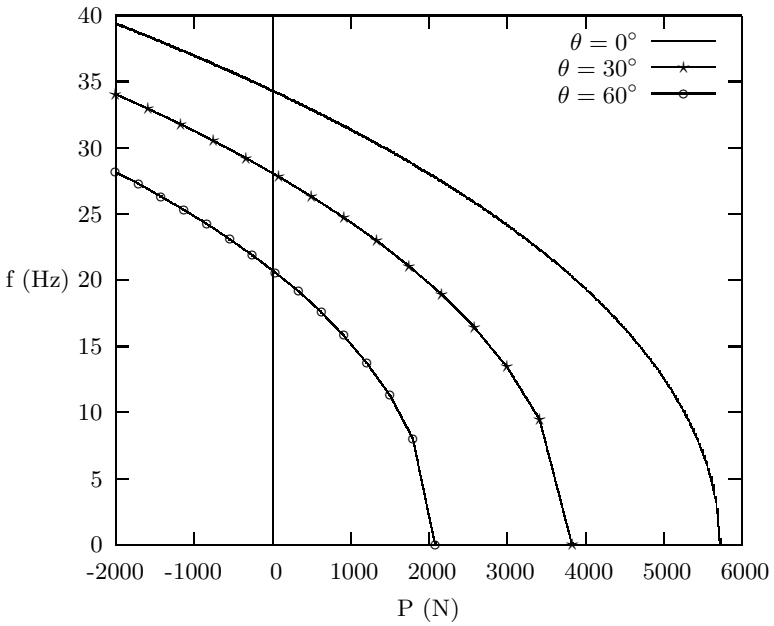

FIG. 4 The interaction diagram between critical buckling load and fundamental natural frequency of a cantilever composite beam with the fiber angle 0°, 30° and 60° in the flanges and web.

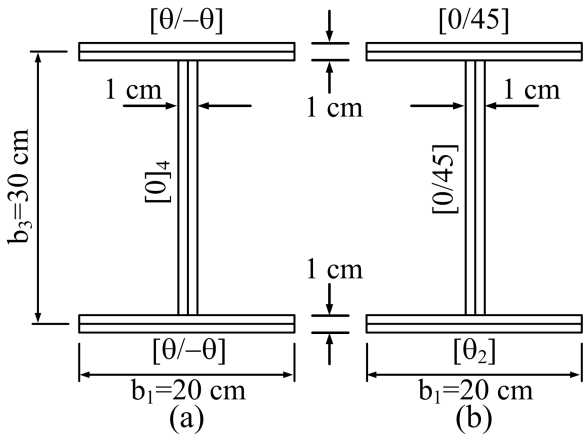

FIG. 5 Geometry and stacking sequences of thin-walled composite I-beam.

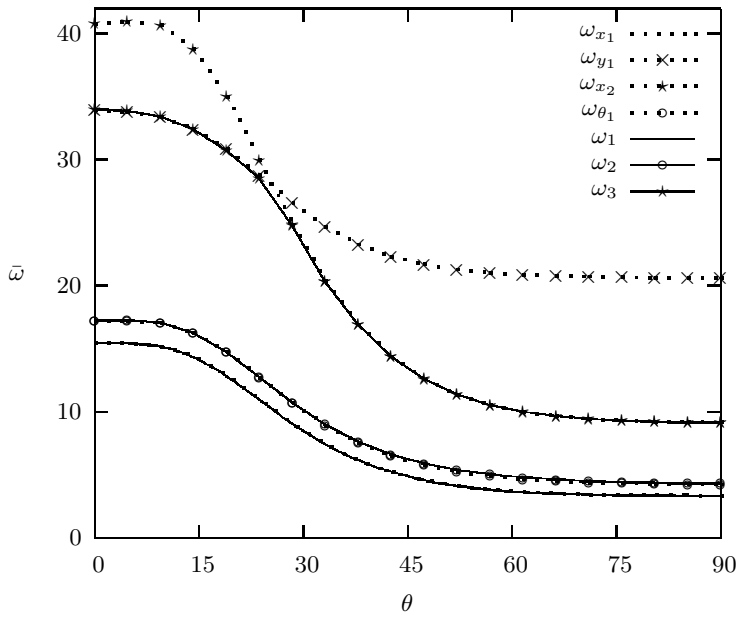

FIG. 6 Variation of the lowest three nondimensional natural frequencies with respect to fiber angle change in the flanges of a clamped composite beam with $l/b_3 = 20$.

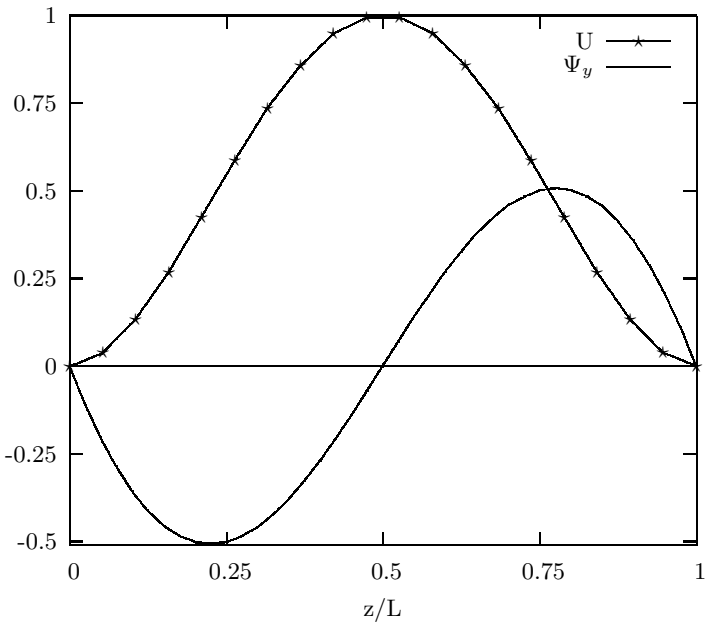

FIG. 7 Mode shapes of the flexural and corresponding shearing components for the first mode $\omega_1 = 8.471$ of a clamped composite beam with the fiber angle 30° in the flanges with $l/b_3 = 20$.

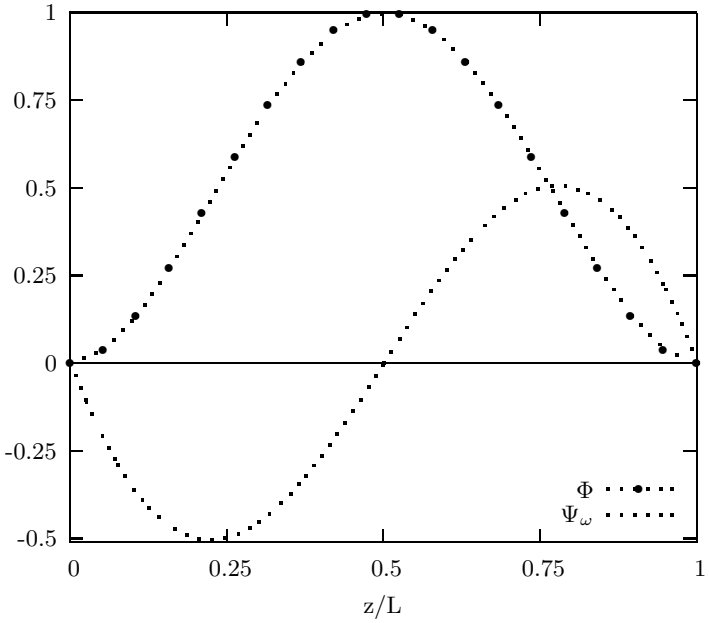

FIG. 8 Mode shapes of the torsional and corresponding shearing components for the second mode $\omega_2 = 10.092$ of a clamped composite beam with the fiber angle 30° in the flanges with $l/b_3 = 20$.

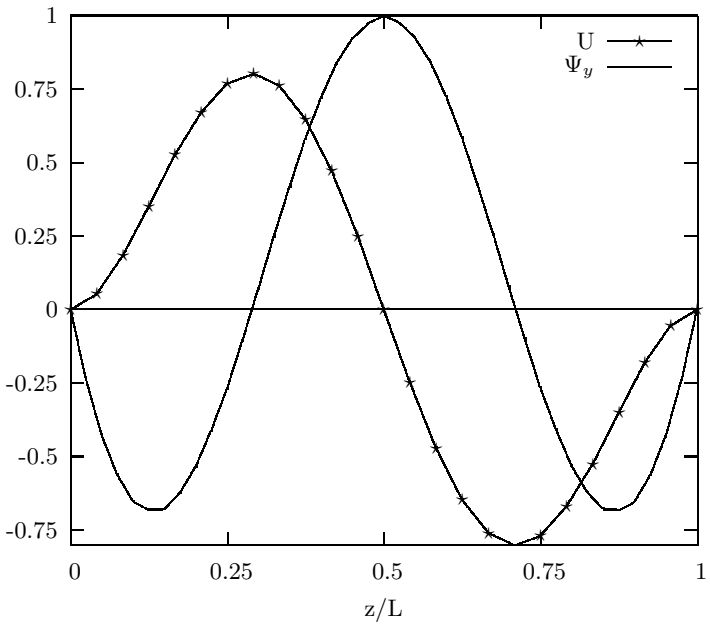

FIG. 9 Mode shapes of the flexural and corresponding shearing components for the third mode $\omega_3 = 23.209$ of a clamped composite beam with the fiber angle 30° in the flanges with $l/b_3 = 20$.

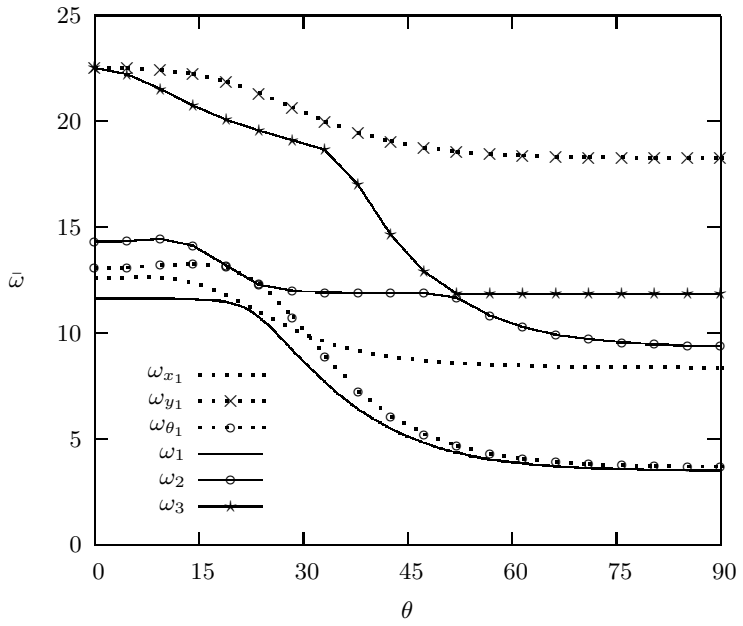

FIG. 10 Variation of the lowest three nondimensional natural frequencies with respect to fiber angle change in the bottom flange of a clamped composite beam with $l/b_3 = 10$.

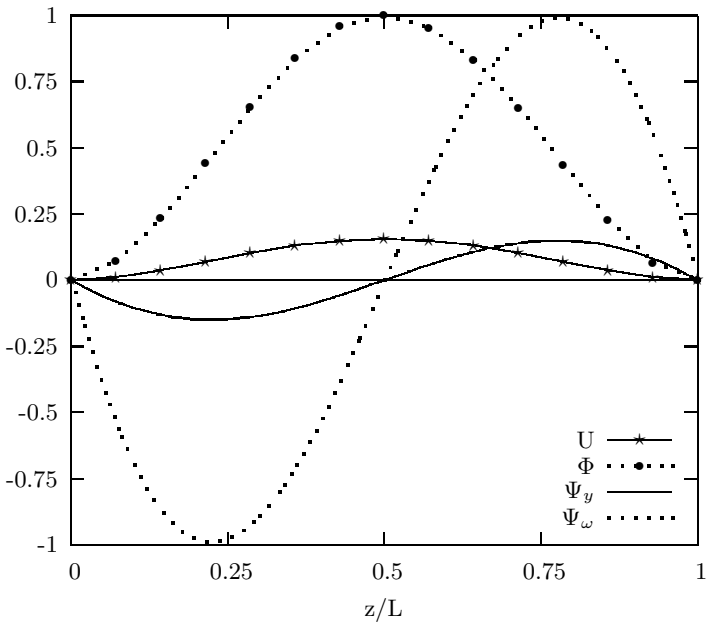

FIG. 11 Mode shapes of the flexural, torsional and corresponding shearing components for the first mode $\omega_1 = 8.678$ of a clamped composite beam with the fiber angle 30° in the bottom flange with $l/b_3 = 10$.

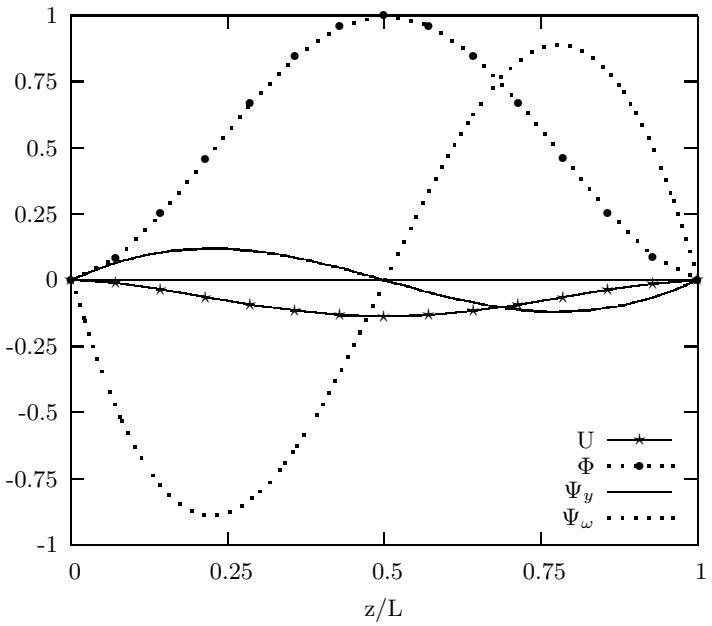

FIG. 12 Mode shapes of the flexural, torsional and corresponding shearing components for the second mode $\omega_2 = 11.966$ of a clamped composite beam with the fiber angle 30° in the bottom flange with $l/b_3 = 10$.

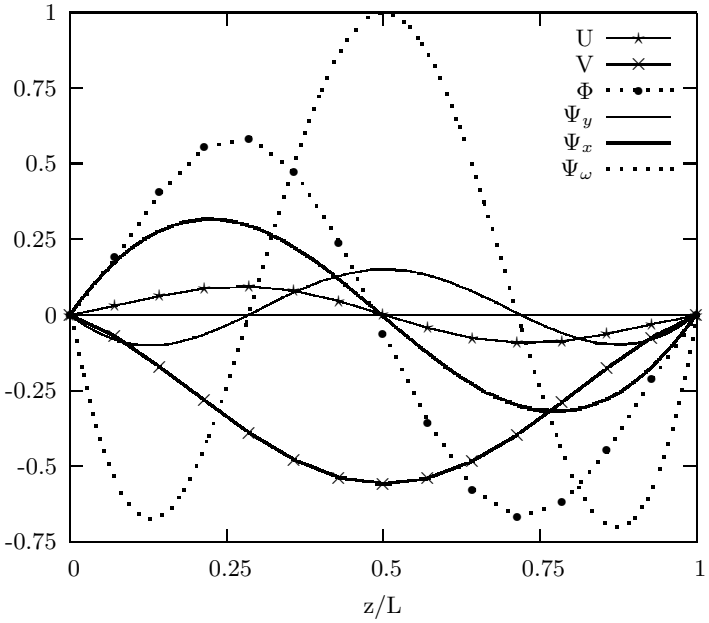

FIG. 13 Mode shapes of the flexural, torsional and corresponding shearing components for the third mode $\omega_3 = 18.980$ of a clamped composite beam with the fiber angle 30° in the bottom flange with $l/b_3 = 10$.